RSC Advances




ROYAL SOCIETY OF CHEMISTRY

www.rsc.org/advances

Journal Name ARTICLE

Received 00th January 20xx,
Accepted 00th January 20xx

DOI: 10.1039/x0xx00000x

www.rsc.org/

# Controlling the self-assembly and optical properties of gold nanoclusters and gold nanoparticles biomineralized with Bovine Serum Albumin

Birgitte H. McDonagh,[a] Gurvinder Singh,[b] Sulalit Bandyopadhyay,[a] Sina M. Lystvet,[a] Joseph A. Ryan,[c] Sondre Volden,[a] Eugene Kim,[d] Ioanna Sandvig,[e,f] Axel Sandvig,[f,g] Wilhelm R. Glomm[a, h]

While the size-dependent optical properties of BSA-stabilized gold nanoclusters are well known, the time-dependent growth mechanism remains to be described. Herein, we systematically compare two synthesis methods with and without ascorbic acid, and show that tuning of BSA-stabilized gold nanoclusters (AuNCs) of different sizes can be performed without the aid of an extrinsic reducing agent and with good reproducibility. We also show that adding ascorbic acid yields larger BSA-stabilized gold nanoparticles (AuNPs), and that AuNPs can only form above a threshold gold precursor concentration. Using computed tomography, we describe how these biomineralized AuNPs show size-dependent X-ray attenuation. Growth of BSA-stabilized AuNCs and AuNPs, over a range of gold precursor concentrations, was followed with steady-state fluorescence and UV-vis spectroscopy for one week, constituting the first study of its kind. Based on our results, we propose a mechanism for BSA-stabilization of AuNCs and AuNPs that can further aid in selective growth of discrete AuNCs and AuNPs.

## Introduction

Applications of protein-stabilized gold nanoparticles (AuNPs) and particularly gold nanoclusters (AuNCs) have increased dramatically since the introduction of the latter in 2009. [1] The main feature of nanometer sized gold is their remarkable size-dependent optical properties. [2, 3] The molecular sized AuNCs fluoresce, while AuNPs (>2nm) exhibit localized surface plasmon resonance (LSPR), resulting in absorbance of visible light. [4-7] Stable, biocompatible fluorescent probes with large Stoke's shifts that emit fluorescence in the Near IR (NIR) range are particularly interesting, as emission is outside the emission region typical of biological tissue.

The amount of atoms in AuNCs follows a shell model named the *Jellium model* with the corresponding magic numbers 2, 8, 10, 20, 26, 34, 40. An analogy to the Jellium model is the electronic structure of atoms, in which each shell is stable with an optimal amount of electrons. As the stability of an atom is governed by closed valence shells, so is the stability of magic numbered nanoclusters. [8-10]

The size-dependent fluorescence of AuNCs can be measured using steady-state fluorescence spectroscopy. However, the actual origin of fluorescence is not clear, as it can arise from the metal core, or from interactions between the metal core and surface ligands. [4] Particularly, electron-rich atoms appear to affect the fluorescence intensity in a positive manner. Wu *et al* suggests that this can occur in two ways; either as a charge transfer or direct donation of delocalized ligand electrons. [11] Proteins offer a plethora of energy donating atoms, such as S, N and O, and can therefore collectively enhance the fluorescence intensity via surface interactions if they are used as capping agents.

The blood plasma protein *bovine serum albumin* (BSA) was the first protein shown to synthesize and stabilize AuNCs. [1] BSA is the major transporter of drugs and metals in the body, and as such has a high affinity for metals.[12, 13] BSA is also documented to have an affinity for planar and curved gold surfaces. [14-16]

Biomineralization of gold with BSA can give a range of different-sized AuNCs, which in turn show size-dependent fluorescence. The reduction potential of BSA is also strong enough to synthesize AuNPs, and the surface stability imparted by BSA makes these AuNPs more stable in biological buffers compared to citrate-covered AuNPs (Figure 1 b-d).

AuNCs and AuNPs are increasingly being used for a range of different applications in bioimaging, [17] such as optical labels in drug delivery, [18, 19] diagnostics, [20] and as sensors of heavy metal ions, [21, 22] to mention a few. In particular, applications of colloidal AuNPs with diameters less than 100 nm are emerging as promising contrast agents for Computed Tomography (CT)[23].

[a] Ugelstad Laboratory, Department of Chemical Engineering, Norwegian University of Science and Technology (NTNU), 7491 Trondheim, Norway
[b] Department of Materials Science and Engineering, Norwegian University of Science and Technology (NTNU), N-7491 Trondheim, Norway
[c] Department of Chemistry, Iona College, New Rochelle, New York, USA
[d] Department of Circulation and Medical Imaging, Norwegian University of Science and Technology (NTNU), N-7491 Trondheim, Norway
[e] John Van Geest Centre for Brain Repair, Department of Clinical Neurosciences, University of Cambridge, CB2 OPY Cambridge, UK
[f] Department of Neuroscience, Faculty of Medicine, Norwegian University of Science and Technology (NTNU), N-7491, Trondheim, Norway
[g] Division of Pharmacology and Clinical Neurosciences, Department of Neurosurgery, Umeå University, 901 87 Umeå, Sweden
[h] Sector for Biotechnology and Nanomedicine, SINTEF Materials and Chemistry, Trondheim, Norway

* Corresponding author: Tel: +47-73 55 03 25, fax: +47-73 59 40 80, e-mail: birgitte.h.mcdonagh@ntnu.no,

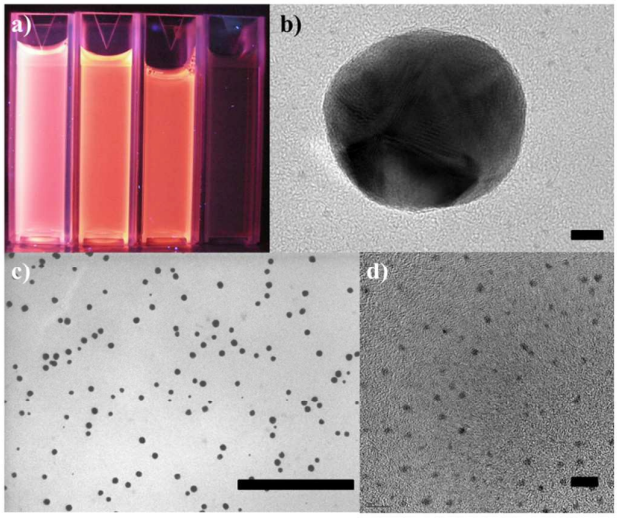


Figure 1: BSA acts as a scaffold for growth of AuNCs and AuNPs. a) Image of BSA-AuNCs and BSA-AuNPs excited with UV-lamp ($\lambda_{ex}$=*365 nm*). The cuvette to the far left had populations of small AuNCs, while the second and third cuvette from the left have populations of larger AuNCs. The dark sample to the far right contains AuNPs which are known to quench fluorescence from AuNCs. b) HR TEM image showing polycrystalline AuNPs that are surrounded by Vis AuNCs (error bar=5nm). Image c) is a TEM image of AuNPs (error bar=500nm), while image d) is an HR TEM image of AuNCs (error bar=5nm).

However, the key to all of these applications remains controlling the size of the AuNCs and AuNPs.

Gold nanoparticles can be prepared *via* several methods. For instance, adding an extrinsic reducing agent such as $NaBH_4$ can be used for preparing gold nano rods, and different aspect ratios can be obtained by changing the concentration of $NaBH_4$. [24] However, recent reports indicate $NaBH_4$ as an extrinsic reducing agent of protein stabilized AuNCs and AuNPs may perturb the solution stability of the protein-AuNC complex due to alterations of the protein structure. This again may be caused by interactions with the $NaBH_4$ and the protein, or that larger gold species are synthesized in the presence of $NaBH_4$, causing the protein to unfold in a greater extent. [25, 26]

The synthesis of AuNCs and AuNPs with BSA has previously been studied with respect to pH,[27] dependences on gold precursor concentrations, [25] and temperature. [1, 22] Ascorbic acid is sometimes added as an extrinsic reducing agent in order to reduce the BSA concentration required,[27] but the effect of ascorbic acid is not completely understood. In fact, studies have shown that ascorbic acid can associate with BSA [28-30] and even quench AuNCs' fluorescence [31] if not removed via *e.g* dialysis. Different incubation times have also been reported, but more thorough studies revealing how the incubation time affects size-tuning of BSA-AuNCs or AuNPs are needed. Protein-directed growth of AuNCs is protein dependent, and addition of an extrinsic reducing agent may be redundant to obtain fluorescent AuNCs. [32]

The mechanism of AuNC growth is still not fully understood despite many reports on the synthesis of BSA-stabilized AuNCs and AuNPs. Since different synthesis protocols and conditions are typically being used between studies, it is problematic to deduce an overall mechanism, which in turn makes it difficult to describe and control the size of BSA-stabilized gold. In order to get a better understanding of the mechanism, there is a need for studies that systematically change one synthesis parameter at a time.

This paper has two aims. First we want to ascribe which parameters are important for self-assembly of gold nanostructures in BSA. This we investigate by varying the concentration of gold precursor, and the presence of an extrinsic reducing agent. The effect of an extrinsic reducing agent (ascorbic acid) is determined by comparing two synthesis methods named the *extrinsic* and *intrinsic* method. The former refers to reduction of gold ions with the aid of ascorbic acid as an extrinsic reducing agent, while the latter method solely depends on the intrinsic reduction potential of BSA. The second aim is to describe a growth mechanism for AuNCs and AuNPs in the BSA scaffold, by using time as the dependent variable.

This paper demonstrates that we can influence the size and thus the optical properties of BSA-AuNCs and AuNPs by varying the above mentioned synthesis parameters. We also describe how synthesis of either BSA-stabilized AuNCs and/or AuNPs can be achieved, and show that size-tunability of AuNCs can be achieved without the presence of ascorbic acid. Finally, we suggest a description of the growth mechanism from AuNCs to AuNPs that can be used to not only get a better understanding of the underlying mechanisms, but also for size-tunability of fluorescent AuNCs or AuNPs with LSPR.

## Experimental

Bovine Serum Albumin (67kDa), hydrogen tetrachloroaureate (III)·3 $H_2O$ (TCAA) and L-ascorbic acid were purchased from Sigma. Stock solutions of BSA (20mg/mL) were freshly prepared in MilliQ-water for each experiment. TCAA (1.18g, 3mmol) was dissolved in MilliQ-water (34.7mL) to make a stock solution (100mM). The TCAA stock solution was then diluted with MilliQ-water to 5, 7.5, 10, 15 and 20mM. BSA from the same batch was used for all samples described. Prior to the reaction, protein TCAA solutions were heated to 37°C. Here, two methods were used for synthesis in the absence and presence of an extrinsic reducing agent, hereafter labelled as the **intrinsic method** and the **extrinsic method**, respectively**. The intrinsic method**: TCAA (2.5mL; 5, 7.5, 10, 15 and 20mM) was added to BSA (2.5mL) at 37°C and stirred (300 rpm) for five minutes. 0.1M NaOH (100-300uL) was added until the solution had a pH of 11. Tyrosine is the amino acid in BSA which is thought to reduce TCAA to NCs and NPs [1]. The phenol group of tyrosine has a $pK_a$ of 10.1,[33] meaning that the synthesis of protein-gold must be performed at high pH-values for maximum reducing capacity. The pH has previously been shown to have an effect on growth of larger NCs, particularly at high pH-values a more prominent growth of large gold NCs has been reported. [27] The reaction was kept in an incubator (37°C) for 1 week followed by dialysis (MWCO: 14kDa) in MilliQ-water. The dialysis was performed with an exchange of the dialyzing solution after two hours, before leaving it overnight to remove excess TCAA. **The extrinsic method:** Ascorbic acid (0.35mg/mL, 50uL) was added immediately after TCAA before pH adjustment. Samples were diluted in MilliQ-water to 1mg BSA/mL before spectroscopic measurements, assuming that the protein concentration did not change with dialysis.

**Steady-state fluorescence spectroscopy** was performed using a Fluorolog-3 HORIBA Jobin Yvon spectrofluorometer with the

excitation wavelengths $\lambda_{ex}$=295nm and $\lambda_{ex}$=370nm. The slit widths were kept at 3 nm and 5 nm, respectively.

**Time-correlated single-photon counting** was performed on the same apparatus as steady-state fluorescence spectroscopy. The protein concentration was 1mg/mL. For measuring tryptophan lifetimes and populations, a 280 nm NanoLED was used as the light source and the emission wavelength was set to $\lambda_{em}$=360nm. The bandpass was kept at 14.5nm.

**UV-visible spectroscopy** was performed on a Shimadzu UV-2401PC spectrophotometer in the range 200-800nm. The data were analyzed using UVProbe2.1 software.

**X-ray photoelectron spectroscopy (XPS)** analyses were performed using a Kratos Axis Ultra DLD spectrometer (Kratos Analytical, UK), equipped with a monochromatized aluminum X-ray source (Al, hυ = 1486.6 eV) operating at 10 mA and 15 kV (150 W). A hybrid lens (electrostatic and magnetic) mode was employed along with an analysis area of approximately 300 µm X 700 µm. Survey spectra were collected over the range of 0-1100 eV binding energy with an analyzer pass energy of 160 eV, and high resolution spectra of Au 4f were obtained with an analyzer pass energy of 20 eV. XPS data were processed with Casa XPS software (Casa Software Ltd., UK).

**High-resolution inductive coupled plasma-mass spectrometry (ICP-MS)** measurements were performed on an ELEMENT 2 from Thermo Electronics with $ArCH_4$ plasma and tested against three blanks. Samples were autoclaved under high pressure with an UltraClave (Milestone) in 50% $HNO_3$ (v/v) at 80°C.

**High resolution transmission electron microscopy (HR-TEM)** images were acquired on a JEOL JEM-2100 (200 kV). The samples were prepared by depositing a few drops of nanoparticles or nanoclusters suspension on a copper grid coated with amorphous carbon layer, and allowed to dry prior to imaging

**X-ray powder diffraction (XRD)** patterns of lyophilized BSA-AuNPs and BSA- AuNCs were obtained from a Bruker DaVinci2 diffractometer using Cu Kα (λ= 1.54056 °A) in the 2θ range with 10–75 degree.

**Computed tomography (CT)** imaging was performed with a Skyscan 1176 micro-CT scanner (Bruker micro-CT, Kontich, BE). Samples of BSA-AuNPs were dialysed against phosphate buffered saline (pH=7.4) before measurements. A phantom consisting of three 0.3 ml centrifuge tubes filled with saline and two BSA-AuNP solutions with concentrations of 15 mg/ml and 30 mg/ml was scanned using the following parameters: 0.5 mm Al filter, 50 kVp, 500 µA, 63 ms exposure, 5 averages, 0.7° rotation step, 180° rotation, 35 µm voxel size. Another, similar phantom containing three samples of BSA-AuNPs (20mg/mL) with different average sizes (6nm, 26nm and 36nm) were scanned with the same imaging parameters. The central 20 slices were reconstructed using the Feldkamp cone-beam reconstruction algorithm to measure the attenuation coefficients (AC) of each suspension. Regions of interest (ROI) were
defined around the inner circumference of each tube in each image slice. The means and standard deviations (s.d) of the ACs within the ROIs were computed.

## Results and Discussion

Immediately after adjusting the pH to 11 for the BSA-TCAA mixture, the solutions changed colour from yellow to orange, brown or red, depending on the amount of TCAA added. After one week incubation time, the most prominent colour change was observed for samples incubated with the highest concentration of TCAA, going from red to dark purple. This change in colour is attributed to AuNPs (>2nm) large enough to exhibit LSPR. [4]

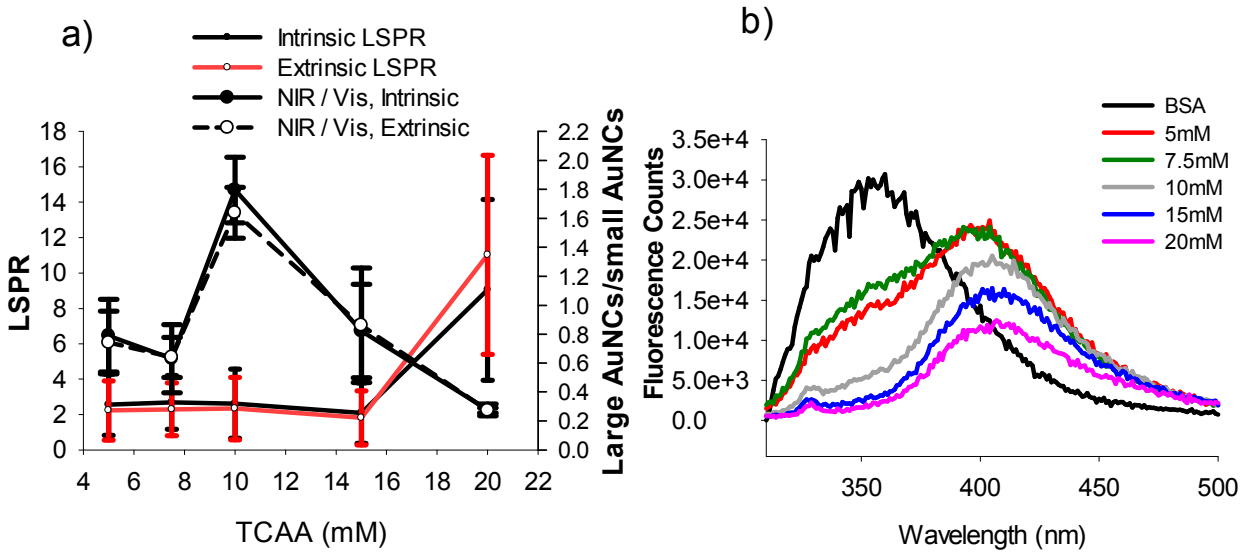


Figure 2: Integrals of a) LSPR absorption peak (500-600 nm) as a function of TCAA synthesized *via* intrinsic and extrinsic method. The integrals of the fluorescence emission ($\lambda_{ex}$=370 nm) of NIR AuNCs (560-730 nm) and Vis AuNCs (385-540 nm) was calculated. The integral of the NIR AuNCs was divided by the integral of Vis AuNCs to show the relative growth of the two sizes of AuNCs. This was done for both the intrinsic and the extrinsic protocol. b) Changes in Trp emission spectra ($\lambda_{ex}$=295 nm) as a function of gold precursor (TCAA).

LSPR appears when the frequency of the incident light matches the oscillation frequency of the surface electrons, relative to the positively charged metallic lattice, leading to an enhancement in the amplitude. [4-7] AuNPs with a dark purple color show an intense UV-visible light extinction band centered at 520nm (Figure S1). Under the conditions reported here, we found that there is a threshold for appearance of AuNPs that lies in between 15 and 20 mM TCAA (Figure 2a). Larger AuNPs were formed when ascorbic acid was added, implying that ascorbic acid contribute to the reduction of TCAA. This is in agreement with earlier studies (see e.g. Le Guèvel[27]) and is also expected, as the presence of an extrinsic reducing agent lowers the energy barrier towards nucleation and growth of nano crystals. The presence of AuNPs was confirmed with HR-TEM (Figure 1b and c), and crystallinity was observed with X-ray powder diffraction (Figure S4), and is also in accordance with values determined in previous studies. [34, 35]

**Size of BSA-gold is dependent on gold precursor concentration**

In contrast to AuNPs, AuNCs have discrete electronic structures such as HOMO-LUMO band gap openings with transitions smaller than the Fermi wavelength.[4] This results in molecule-like properties such as size-dependent fluorescence (Figure 1a). [36, 37] AuNCs vary in size from 0.2nm to 2nm, which for gold corresponds to a few atoms up to several hundreds of atoms. [2, 38] The amount of gold atoms in AuNCs likely follows the Jellium model, which describes clusters as being of a magic number of atoms (=2, 8, 13, 25, 38, 55…). Populations of AuNCs can be described by fluorescence spectroscopy. AuNCs are excited at 370 nm ($\lambda_{ex}$*=370nm)* and emit at 450 nm and 600-700 nm, depending on their size (Figure S2). Here, the peak at 450 nm is attributed to populations of smaller AuNCs ($Au_8$, $Au_{13}$ *etc*) which are hereon referred to as Vis AuNCs as they emit in the visible region of the electromagnetic spectrum. The fluorescence between 600 and 700nm is attributed to populations of larger AuNCs ($Au_{25}$), hereon referred to as NIR AuNCs. [1, 27]

The large NIR fluorescence intensity observed for AuNCs at 10mM TCAA might be a result of a metal-to-ligand/ligand-to-metal charge-transfer (ML/LMCT) complex that is formed between the protein and the NIR AuNCs. This is hypothesized to enhance the fluorescence intensities. However, in an ML/LMCT complex there is an exchange of electrons either from the metal to the protein or *vice versa*. If this was largely the case, either the protein or the AuNCs would be oxidized/reduced, which would destabilize the suspension with time. Thus, as the suspensions were very stable over long time periods (>1 year), it is more likely that the high fluorescence intensity from NIR AuNCs is caused by capping of BSA. This would in turn cause shielding of the AuNC from water, which further would give a more intense fluorescence emission.

The AuNCs prepared with the intrinsic method show the same intensity and reproducibility as samples synthesized with ascorbic acid. Given that the concentration of ascorbic acid used was in accordance with previous literature. [27, 39] This finding suggests that the concentration of ascorbic acid used here does not significantly aid BSA in reducing $Au^{3+}$ to AuNCs. At low concentrations, there are predominantly Vis clusters present, but as the concentration of TCAA increases, so does the population of NIR AuNCs (Figure 2b). However, as AuNPs emerge, detecting the presence of AuNCs with fluorescence spectroscopy becomes highly complex as the interactions between colloids and fluorophores can involve resonance energy transfer and quenching. [7] The Vis AuNCs on the other hand, seem to be unaffected by the presence of AuNPs as their fluorescence intensities continue to increase with TCAA concentration. The most probable reason for this is that the emission from Vis AuNCs is out of range of AuNP quenching or that Vis AuNCs are too far away from AuNPs. Appearance of AuNPs occurs only at high concentrations of TCAA (20mM, Figure 2a). At 20mM TCAA, there is a substantial decrease in the emission of NIR AuNCs (Figure 2b), as well as a bathochromic shift of the emission peak at 650 nm (Figure S2). This could be caused by NIR AuNCs being quenched by AuNPs, coalescence of NIR AuNCs into AuNPs, or a combination of both.

With X-ray photoelectron spectroscopy, the binding energy of surface photoelectrons can be measured. Higher binding energies indicate that the surface electrons are more associated with the metal, and less prone to movement between metallic surfaces. [27, 40, 41] A lower binding energy means that the surface electrons have less affinity to the metallic core. Here, BSA-AuNCs show gold peaks at 80.1 and 83.8eV, while BSA-AuNPs show a shift to higher binding energies (84.9eV and 81.2eV, respectively. Figure S5). The peaks for BSA-AuNPs are also broadened, and show higher intensities compared to the BSA-AuNCs. Because XPS can only detect elemental compositions of surfaces down to 10nm[42-44], a shift to higher binding energies with higher concentrations of TCAA, means that Vis AuNCs are present on the surface of the protein. It also implies that NIR AuNCs are not on the surface and (i) has either coalesced into NPs or (ii) are buried in BSA. The XPS spectra, combined with HR TEM images (Figure 1b and c) strongly suggests that AuNCs coexist with AuNPs, and imply that the AuNPs are covered with BSA-AuNCs as passivating ligands.

**Tryptophan emission is altered due to size of BSA-stabilized AuNCs and AuNPs.**

BSA is a very flexible protein and can undergo major conformational changes without denaturation.[45-47] The flexibility is important for the amount of gold that can be loaded onto the protein backbone. Changes in the conformation of BSA can be described by steady-state fluorescence spectroscopy by exciting the amino acid tryptophan (Trp). The indole ring in Trp is the dominant fluorophore in proteins, absorbing light near 295 nm and emitting near 340 nm.[48, 49] Indole is very sensitive to solvent polarity and can reveal the location of tryptophan residues in proteins. Typically, emissions from exposed Trp residues are red-shifted, while buried Trp residues will have a blue-shifted emission.[7, 50] Stoke's shifts and quenching of tryptophan emission is usually explained by an exposure to the aqueous environment. [7, 49, 51] BSA has two tryptophan residues; one situated in a hydrophobic pocket (Trp213) while the other is situated on the surface (Trp134).[47] Because Trp213 is hidden inside native BSA, the tryptophan emission ($\lambda_{ex}$ *=295 nm*) is thought to be dominated by Trp134. Therefore, any changes in the emission are ascribed to structural changes in the protein. [25, 49, 52] Steady-state fluorescence spectroscopy was used to measure Trp emission in BSA containing different sizes and populations of nano-sized gold. Trp134 in native BSA has an emission maximum at approximately 350 nm in water. This maximum was steadily quenched and shifted towards longer wavelengths as the size of the nano-sized gold increased (Figure 2b). No differences between the intrinsic and extrinsic methods were observed with TCAA concentrations above 5mM. However, the emission of BSA incubated with ascorbic acid had the largest standard deviations (Figure S3), which could imply that not all of

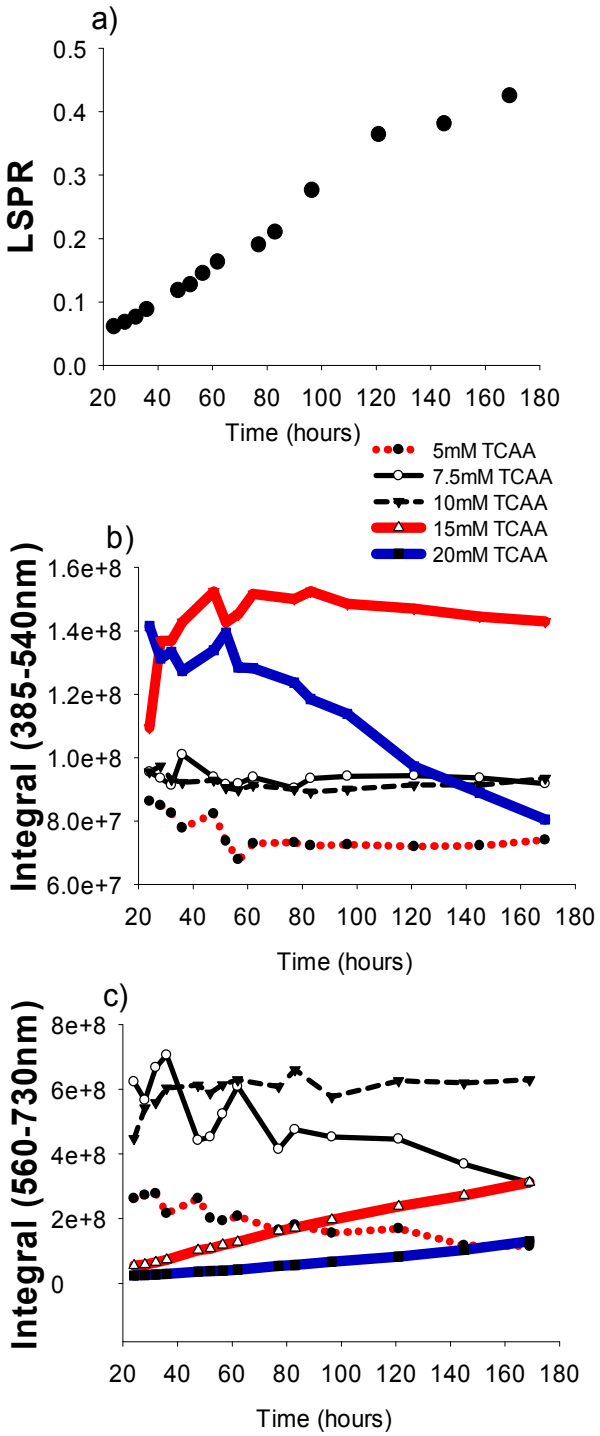


Figure 3: Graph a) shows the LSPR intensity at 520nm as a function of time for the sample incubated with 20mM TCAA. No LSPR-band was observed for any other samples. Graph b) shows the integral of the emission peak for the Vis AuNCs (385-540 nm) after subtracting the signal of native BSA. Graph c) show the integral of the emission peaks of NIR AuNCs (560-730 nm) after subtracting the signal of native BSA. Both graph b and c are shown as a function of time. The lines for 15 and 20 mM TCAA have been highlighted as they show the most consistent changes.

the ascorbic acid was removed *via* dialysis because it was bound to the protein.

The Trp emission (Figure 2b) curve has an inflection point approximately at 360 nm, which is best observed with the 5mM curve (red). As AuNCs are excited at 370 nm, it is likely that the decrease in Trp emission is not only caused by exposure to the surface, but also by quenching of adjacent AuNCs. After 360nm, the Trp emission intensity slowly increases to 450 nm, before it decreases again.

The whole emission profile of BSA is drastically altered from TCAA concentrations of 10mM and above, meaning that the protein has undergone large conformational changes. At 10mM TCAA there is a dramatic change in the Trp emission from 300 to 400 nm. At this particular concentration of TCAA, the highest ratio of NIR AuNCs was determined (Figure 2a). This means that with a bigger population of NIR AuNCs, the probability that a quencher is adjacent to a Trp residue increases. However, Trp quenching cannot only be explained by AuNC quenching alone. With increased population of nano-sized gold, BSA unfolds and exposes Trp134 to water, which will be a large contributor to quenching.[25] Unfolding also leads to exposure of the buried tryptophan residue (Trp213), which emission emerge at ~320nm for samples containing 10-20mM TCAA.

From time-correlated single photon spectroscopy (TCSPC) a large difference in the Trp lifetimes of native BSA and BSA with AuNPs (20mM TCAA) was detected (Table S2). This indicates that the fluorophore on average spends less time in the excited state, which is probably caused by an increased exposure to water or energy transfer to BSA-gold, or a combination of the two. [25]

Combining the TCSPC data with steady-state fluorescence data, we ascribe quenching of Trp emission as concomitant effect of increased size of BSA-AuNCs/AuNPs. Interestingly, even though the Trp emission reveals large structural changes in BSA, the BSA-AuNP solution did not show any signs of aggregation after 12 months of storage. This means that the conformational changes induced by nano-sized gold are not large enough to severely denature BSA, and compromise its solution stability. The long shelf-life of BSA-AuNP suspensions enhances their utility *e.g* in sensing and imaging applications.[53-55]

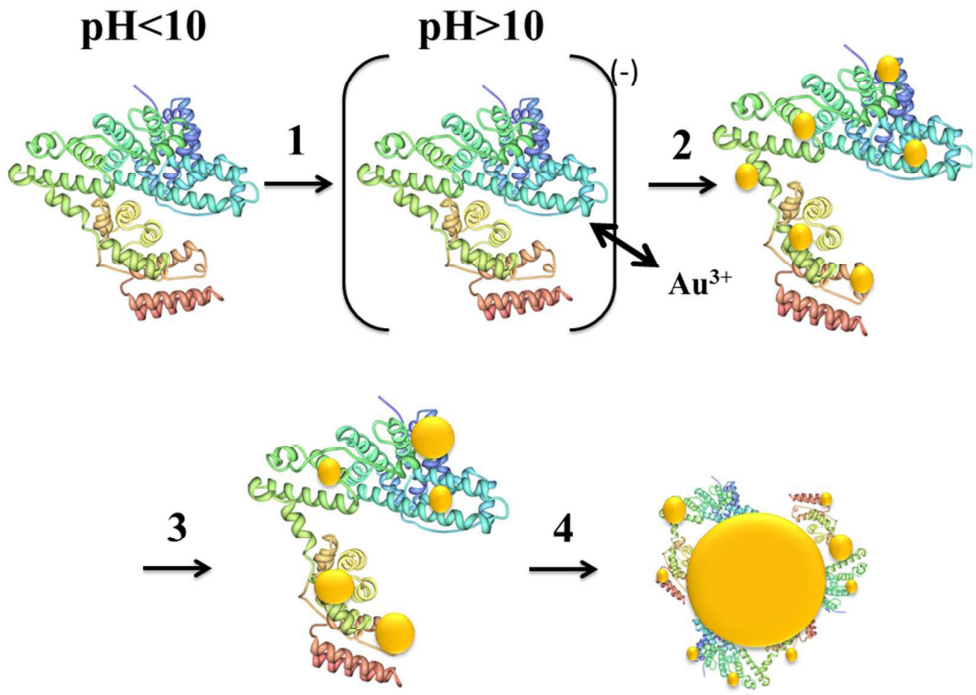


Figure 4: Proposed mechanism for growth of AuNPs stabilized by BSA. 1) Increasing the pH to above 10 causes BSA to be negatively charged which induces electrostatic interactions with the gold ions. 2) Vis AuNCs that emit in the visible region of the EM spectrum start to form, 3) and depending on time and concentration of TCAA, larger NIR AuNCs and 4) AuNPs are formed via a shuffling of NIR AuNCs. It should be noted that the structure of the denatured protein is used only as illustration, and not as an accurate description of the conformation

**Proposed mechanism for biomineralization of AuNCs and AuNPs**

We have established that changing the ratio of BSA/TCAA yields different populations of nanometer-sized gold, and that ascorbic acid is not needed for synthesis of AuNCs, but that it is beneficial for biomineralization of AuNPs.

The incubation time for the samples prepared above was one week, [25, 32] which is much longer compared to the original synthesis of 12 hours.[1] 12 hours incubation time is also reported by several others,[39, 56-59] but overnight,[60] 15 hours,[22] 5 hours,[27, 39] and 2 hours[25] have also been used for BSA-AuNCs synthesis. The different incubation times yield different populations of AuNCs, revealing that the synthesis is highly time-dependent.

We wanted to elucidate the time-dependent changes in the protein and what appears to be a dynamic interchange between Vis and NIR AuNCs that could give further insight to the nucleation and growth processes. In order to address this issue, biomineralization of AuNCs and AuNPs with BSA was followed for one week.

In Figure 4 we have illustrated what we suggest as the self-assembly mechanism of BSA-stabilized AuNCs and AuNPs. Initially, the pH is raised to above 10 so that BSA becomes negatively charged (step 1, Figure 4). [61] Positively charged gold ions are then electrostatically attracted to BSA, particularly in areas rich in tyrosine and histidine which are the major reducing amino acids. Once the local concentration of gold ions is high enough, nucleation occurs (step 2), and further growth of AuNCs is caused by an increased influx of gold ions, or due to coalescence, or both (step 3). Chaudhari *et al* points to that the evolution of AuNCs in protein backbones are facilitated by the flexibility and unfolding of the protein, [62] which is consistent with what we report here. If the concentration of TCAA is high enough, AuNPs are synthesized most likely due to coalescence of several proteins surrounding an AuNP core (step 4), consistent with the general mechanism described by Volden *et.al.* [32]

The initial electrostatic interactions of $Au^{3+}$ ions will favor nucleation at sites high in concentration of negatively charged amino acids. This in turn suggests that nucleation is likely to take place in these regions as well. Indeed, the reduction in Trp emission observed in Figure 2b (5 and 7.5mM TCAA) could be an effect of exactly that. Nucleation that takes place close to a dominating fluorophore would in turn cause quenching, as AuNCs can interact with the emitted photons from Trp213. This also leans towards the fact that nucleation does not take place in the central hydrophobic regions of the protein, as Trp134 emission is not quenched with increased concentration of gold ions (Figure 2b, 10-20 mM TCAA, Trp peak at 320 nm).

Biomineralization of AuNPs is highly time-dependent, with AuNPs of 20 nm occurring after one week of incubation with BSA, but only at high concentrations of TCAA (20 mM, Figure 3a). Synthesis of AuNCs, however, is not equally linear and straight-forward. Up until 60 hours of incubation time, there are large fluctuations in the populations of Vis AuNCs (Figure 3b). Beyond 60 hours, the population sizes decrease but at different rates. The largest changes are seen with the highest concentration of TCAA, which seem to inversely follow the growth of AuNPs (Figure 3a), suggesting increased quenching of AuNCs with appearance of

AuNPs. For samples containing 15 and 20 mM TCAA, decrease in populations of Vis AuNCs is followed by growth of NIR AuNCs, which is not equally observed for the other samples (Figure 3c). This suggests that Vis AuNCs coalesce into NIR AuNCs, and that this is most prominent when high concentrations of TCAA are added. For samples containing 5-10 mM TCAA, there are particularly large fluctuations in the emissions for NIR AuNCs up until approximately 100 hours. During the time course of the experiment, peak shoulders were consistently observed for the NIR AuNCs, but not for the Vis AuNCs. Emission peaks of AuNCs that broaden and have shoulders indicate that different discrete AuNC populations of magic Jellium numbers are present in the protein backbone.[25, 63] This means that there are at least two populations of NIR AuNCs present, and that the population sizes are changing based on the available amount of $Au^{3+}$. The spectral line shape of 7.5mM TCAA is particularly interesting (Figure S9). In the beginning of the reaction, the peak at 650 nm has a shoulder that lies to the left, but after 62 hours of reaction time, the shoulder has shifted to the right, meaning that AuNCs of higher magic Jellium numbers are formed. At 62 hours, there are minor changes in the population of Vis AuNCs, which could mean that growth of larger AuNCs is caused by an influx of $Au^{3+}$ to the protein surface from the bulk, rather than coalescence of Vis AuNCs as the latter would have revealed a decrease in the population of Vis AuNCs.

It is very important to point out that emission of AuNCs tend to be higher at short incubation times, with the exception of NIR AuNCs for samples containing 15 and 20 mM TCAA. This suggests that synthesis of AuNCs with high quantum yields should be performed with incubation times below 40 hours.

Volden *et al* also points to the flexibility of the protein as a key feature for synthesis of AuNCs. The Trp emission was also followed with time, and revealed how BSA rapidly undergoes conformational changes during the biomineralization process. The Trp emission line shape did not change after 24 hours incubation time (Figure S10) but had the same shape as that observed after one week (Figure 2b). With the sample prepared at 20 mM TCAA, the changes during the week were less prominent, which indicates that the protein has less chances of conformational changes due to the NIR AuNCs and AuNPs present in its backbone. However, changes to the emission of the other samples were observed and is worth highlighting. The samples containing 5-15 mM TCAA actually showed an increase in the Trp emission at the end of the week compared to 24 hours. Increased emission of Trp represents a refolding of the BSA with time. As size and amount of AuNCs grow, BSA is forced to stretch and expose hydrophobic pockets to the aqueous environment. At some point, the unfavorable interactions between hydrophobic residues and water will force the protein to change conformation. Refolding of BSA may in turn bring Vis AuNCs closer to each other, which would increase the probability of coalescence into NIR AuNCs. The concomitant decrease in the Vis AuNCs (Figure 3b) could therefore be an effect of refolding of BSA that is greater with time. It is likely that NIR AuNCs also remain in the protein backbone as they can be visualized with HR TEM (Figure 1 c) and measured with steady-state fluorescence spectroscopy.

The easy size tuning, low toxicity, excellent stability, and optical properties of BSA-stabilized AuNCs and AuNPs render these constructs highly useful in several applications. For instance, we have initial data suggesting that BSA-AuNPs show size-dependent X-ray attenuation, which can be used in computed tomography (Figure S7).

## Conclusions

We have systematically compared the role of BSA in reducing $Au^{3+}$ to AuNCs of different sizes using two different synthesis protocols – with and without the addition of ascorbic acid as an extrinsic reducing agent. Our results demonstrate that the presence of ascorbic acid plays a minor role in the formation of BSA-AuNCs, but that ascorbic acid yields larger BSA-AuNPs. We have also shown that the size of BSA-AuNCs and BSA-AuNPs is in turn dependent on the TCAA concentration and the incubation time. BSA is a robust and flexible protein that can carry a substantial amount of AuNCs in its backbone, and can even stabilize AuNPs without denaturing, showing great solution stability even after one year. We suggest that gold nanoparticles grow at the expense of NIR nanoclusters, and that this is enabled by the flexibility of BSA. We have also shown that at lower TCAA concentrations, Vis and NIR AuNCs co-exist in the protein backbone, and that this ratio is tunable. The mechanism described here can be easily applied for size-selection of BSA stabilized AuNCs and AuNPs, tuning the growth towards different applications.

## Acknowledgements

The authors acknowledge the Department of Chemical Engineering, NTNU, for financial support. Sulalit Bandyopadhyay acknowledges the Faculty of Natural Sciences and Technology, NTNU for financial support. Gurvinder Singh thanks NTNU Nanolab for providing instrumentation facilities. The Research Council of Norway is acknowledged for the support to the Norwegian Micro- and Nano-Fabrication Facility, NorFab (197411/V30). Axel Sandvig and Ioanna Sandvig acknowledge financial support by the Central Norway Regional Health Authority NTNU Liaison Committee. Finally, acknowledgements are given to Moreland *et al*[64] for providing necessary software for preparation of 3D imaging of BSA.

## References

1. Xie, J.; Zheng, Y.; Ying, J. Y. *J. Am. Chem. Soc.* **2009,** 131, (3), 888-889.
2. Le Guevel, X. *IEEE Journal on Selected Topics in Quantum Electronics* **2014,** 20, (3).
3. Qu, X.; Li, Y.; Li, L.; Wang, Y.; Liang, J.; Liang, J. *Journal of Nanomaterials* **2015,** 2015, 23.
4. Qian, H.; Zhu, M.; Wu, Z.; Jin, R. *Acc. Chem. Res.* **2012,** 45, (9), 1470-1479.
5. Jain, P. K.; Huang, X.; El-Sayed, I. H.; El-Sayed, M. A. *Acc. Chem. Res.* **2008,** 41, (12), 1578-1586.
6. Jain, P. K.; ElSayed, I. H.; El-Sayed, M. A. *Nano Today* **2007,** 2, (1), 18-29.
7. Lakowicz, J. R., *Principles of Fluorescence Spectroscopy*. 3 ed.; Springer: USA, 2006.
8. de Heer, W. A. *Rev. Mod. Phys.* **1993,** 65, (3), 611-676.
9. Janssens, E.; Neukermans, S.; Lievens, P. *Curr. Opin. Solid State Mater. Sci.* **2004,** 8, (3–4), 185-193.
10. Reber, A. C.; Khanna, S. N.; Castleman Jr, A. W., Chapter 9 - Superatoms: From Motifs to Materials. In *Science and Technology of Atomic, Molecular, Condensed Matter & Biological Systems*, Purusottam, J.; Castleman, A. W., Eds. Elsevier: 2010; Vol. Volume 1, pp 365-381.
11. Wu, Z.; Jin, R. *Nano Lett.* **2010,** 10, (7), 2568-2573.

12. Bal, W.; Christodoulou, J.; Sadler, P. J.; Tucker, A. *J. Inorg. Biochem.* **1998,** 70, (1), 33-39.
13. Sadler, P. J.; Viles, J. H. *Inorg. Chem.* **1996,** 35, (15), 4490-4496.
14. Ni Dhubhghaill, O. M.; Sadler, P. J.; Tucker, A. *J. Am. Chem. Soc.* **1992,** 114, (3), 1118-1120.
15. Glomm, W. R.; Halskau Jr, Ø.; Hanneseth, A. M. D.; Volden, S. *Journal of Physical Chemistry B* **2007,** 111, (51), 14329-14345.
16. Brewer, S. H.; Glomm, W. R.; Johnson, M. C.; Knag, M. K.; Franzen, S. *Langmuir* **2005,** 21, (20), 9303-9307.
17. Sun, C.; Yang, H.; Yuan, Y.; Tian, X.; Wang, L.; Guo, Y.; Xu, L.; Lei, J.; Gao, N.; Anderson, G. J.; Liang, X. J.; Chen, C.; Zhao, Y.; Nie, G. *J. Am. Chem. Soc.* **2011,** 133, (22), 8617-8624.
18. Lu, W.; Zhang, Y.; Tan, Y. Z.; Hu, K. L.; Jiang, X. G.; Fu, S. K. *J. Controlled Release* **2005,** 107, (3), 428-448.
19. Khandelia, R.; Jaiswal, A.; Ghosh, S. S.; Chattopadhyay, A. *Small* **2013,** 9, (20), 3494-3505.
20. Retnakumari, A.; Jayasimhan, J.; Chandran, P.; Menon, D.; Nair, S.; Mony, U.; Koyakutty, M. *Nanotechnology* **2011,** 22, (28).
21. Xie, J.; Zheng, Y.; Ying, J. Y. *Chem. Commun.* **2010,** 46, (6), 961-963.
22. Chen, P. C.; Chiang, C. K.; Chang, H. T. *J. Nanopart. Res.* **2013,** 15, (1).
23. Cole, L. E.; Ross, R. D.; Tilley, J. M.; Vargo-Gogola, T.; Roeder, R. K. *Nanomedicine* **2015,** 10, (2), 321-341.
24. Zhang, L.; Xia, K.; Lu, Z.; Li, G.; Chen, J.; Deng, Y.; Li, S.; Zhou, F.; He, N. *Chem. Mater.* **2014,** 26, (5), 1794-1798.
25. Lystvet, S. M.; Volden, S.; Singh, G.; Yasuda, M.; Halskau, O.; Glomm, W. R. *RSC Advances* **2013,** 3, (2), 482-495.
26. McDonagh, B. H.; Volden, S.; Lystvet, S. M.; Singh, G.; Ese, M. H.; Ryan, J. A.; Lindgren, M.; Sandvig, A.; Sandvig, I.; Glomm, W. R. *Nanoscale* **2015,** 7, (17), 8062-70.
27. Le Guével, X.; Hötzer, B.; Jung, G.; Hollemeyer, K.; Trouillet, V.; Schneider, M. *J. Phys. Chem. C* **2011,** 115, (22), 10955-10963.
28. Nafisi, S.; Bagheri Sadeghi, G.; Panahyab, A. *J. Photochem. Photobiol. B: Biol.* **2011,** 105, (3), 198-202.
29. Sun, L.; Zhang, J.; Liu, K. *Anal. Lett.* **2007,** 40, (16), 3050-3059.
30. Tukamoto, T.; Ozeki, S.; Hattori, F.; Ishida, T. *Chem. Pharm. Bull.* **1974,** 22, (2), 385-389.
31. Wang, X.; Wu, P.; Hou, X.; Lv, Y. *The Analyst* **2013,** 138, (1), 229-233.
32. Volden, S.; Lystvet, S. M.; Halskau, Ø.; Glomm, W. R. *RSC Advances* **2012,** 2, (31), 11704-11711.
33. Nelson, D. L.; Cox, M. M., *Lehninger Principles of Biochemistry*. 5 ed.; W.H Freeman and Company: USA, 2008.
34. Geetha, R.; Ashokkumar, T.; Tamilselvan, S.; Govindaraju, K.; Sadiq, M.; Singaravelu, G. *Cancer Nanotechnol.* **2013,** 4, (4-5), 91-98.
35. Jiao, J.; Zhang, H.; Yu, L.; Wang, X.; Wang, R. *Colloids Surf. Physicochem. Eng. Aspects* **2012,** 408, 1-7.
36. Lin, C. A. J.; Yang, T. Y.; Lee, C. H.; Huang, S. H.; Sperling, R. A.; Zanella, M.; Li, J. K.; Shen, J. L.; Wang, H. H.; Yeh, H. I.; Parak, W. J.; Chang, W. H. *ACS Nano* **2009,** 3, (2), 395-401.
37. Yuan, C. T.; Chou, W. C.; Tang, J.; Lin, C. A.; Chang, W. H.; Shen, J. L.; Chuu, D. S. *Opt. Express* **2009,** 17, (18), 16111-16118.
38. Aikens, C. M. *J. Phys. Chem. Lett.* **2011,** 2, (2), 99-104.
39. Das, T.; Ghosh, P.; Shanavas, M. S.; Maity, A.; Mondal, S.; Purkayastha, P. *Nanoscale* **2012,** 4, (19), 6018-6024.
40. Peters, S.; Peredkov, S.; Neeb, M.; Eberhardt, W.; Al-Hada, M. *Surf. Sci.* **2013,** 608, 129-134.
41. Tanaka, A.; Takeda, Y.; Imamura, M.; Sato, S. *Physical Review B* **2003,** 68, (19), 195415.
42. McArthur, S. L. *Surf. Interface Anal.* **2006,** 38, (11), 1380-1385.
43. Sezen, H.; Suzer, S. *Thin Solid Films* **2013,** 534, 1-11.
44. Hajati, S.; Tougaard, S. *Anal. Bioanal. Chem.* **2010,** 396, (8), 2741-2755.
45. El Kadi, N.; Taulier, N.; Le Huérou, J. Y.; Gindre, M.; Urbach, W.; Nwigwe, I.; Kahn, P. C.; Waks, M. *Biophys. J.* **2006,** 91, (9), 3397-3404.
46. Bloomfield, V. *Biochemistry* **1966,** 5, (2), 684-689.
47. Cao, X. L.; Li, H. W.; Yue, Y.; Wu, Y. *Vib. Spectrosc* **2013,** 65, 186-192.
48. Gelamo, E. L.; Silva, C. H. T. P.; Imasato, H.; Tabak, M. *Biochimica et Biophysica Acta - Protein Structure and Molecular Enzymology* **2002,** 1594, (1), 84-99.
49. Sułkowska, A. *J. Mol. Struct.* **2002,** 614, (1-3), 227-232.
50. Xu, J.; Chen, J.; Toptygin, D.; Tcherkasskaya, O.; Callis, P.; King, J.; Brand, L.; Knutson, J. R. *J. Am. Chem. Soc.* **2009,** 131, (46), 16751-16757.
51. De Paoli Lacerda, S. H.; Park, J. J.; Meuse, C.; Pristinski, D.; Becker, M. L.; Karim, A.; Douglas, J. F. *ACS Nano* **2010,** 4, (1), 365-379.
52. Hierrezuelo, J. M.; Nieto-Ortega, B.; Carnero Ruiz, C. *J. Lumin.* **2014,** 147, 15-22.
53. Vasimalai, N.; John, S. A. *Analytical Methods* **2013,** 5, (20), 5515-5521.
54. Wei, S. C.; Hsu, P. H.; Lee, Y. F.; Lin, Y. W.; Huang, C. C. *ACS Applied Materials and Interfaces* **2012,** 4, (5), 2652-2658.
55. Liu, Z.; Luo, L.; Dong, Y.; Weng, G.; Li, J. *J. Colloid Interface Sci.* **2011,** 363, (1), 182-186.
56. Hu, L.; Han, S.; Parveen, S.; Yuan, Y.; Zhang, L.; Xu, G. *Biosensors Bioelectron.* **2012,** 32, (1), 297-299.
57. Wang, M.; Mei, Q.; Zhang, K.; Zhang, Z. *Analyst* **2012,** 137, (7), 1618-1623.
58. Wang, Y.; Chen, J.; Irudayaraj, J. *ACS Nano* **2011,** 5, (12), 9718-9725.
59. Zhang, M.; Dang, Y. Q.; Liu, T. Y.; Li, H. W.; Wu, Y.; Li, Q.; Wang, K.; Zou, B. *J. Phys. Chem. C* **2013,** 117, (1), 639-647.
60. Raut, S.; Chib, R.; Rich, R.; Shumilov, D.; Gryczynski, Z.; Gryczynski, I. *Nanoscale* **2013,** 5, (8), 3441-3446.
61. Peng, Z. G.; Hidajat, K.; Uddin, M. S. *J. Colloid Interface Sci.* **2004,** 271, (2), 277-283.
62. Chaudhari, K.; Xavier, P. L.; Pradeep, T. *ACS Nano* **2011,** 5, (11), 8816-8827.
63. Zheng, J.; Nicovich, P. R.; Dickson, R. M., Highly fluorescent noble-metal quantum dots. 2007; Vol. 58, pp 409-431.
64. Moreland, J. L.; Gramada, A.; Buzko, O. V.; Zhang, Q.; Bourne, P. E. *BMC Bioinformatics* **2005,** 6.